Analyst

PAPER

View Article Online
View Journal

Cite this: DOI: 10.1039/c9an01664c

A dual-enzyme, micro-band array biosensor based on the electrodeposition of carbon nanotubes embedded in chitosan and nanostructured Au-foams on microfabricated gold band electrodes†

Vuslat B. Juska *[a,b] and Martyn E. Pemble [a,b]

We report the development of a dual-enzyme electrochemical biosensor based on microfabricated gold band array electrodes which were first modified by gold foam (Au-foam) in order to dramatically increase the active surface area. The resulting nanostructured Au-foam deposits then served as a highly porous 3D matrix for the electrodeposition of a nanocomposite film consisting of multi walled carbon nanotubes embedded in a chitosan matrix (CS:MWCNT) designed to provide a conducting, biocompatible and chemically versatile surface suitable for the attachment of a wide range of chemically or biologically active agents. Finally, a dual enzyme mixture of glucose oxidase (GOx) and horseradish peroxidase (HRP) was immobilised onto the CS:MWCNT nanocomposite film surface. It is shown that the resulting sensing platform developed demonstrates excellent analytical performance in terms of glucose detection with a sensitivity of 261.8 μA mM^{-1} cm^{-2} and a reproducibility standard deviation (RSD) of 3.30% as determined over 7 measurements. Furthermore, long term stability studies showed that the electrodes exhibited an effectively unchanged response to glucose detection after some 45 days. The example of glucose detection presented here illustrates the fact that the particular combination of nanostructured materials employed represents a very flexible platform for the attachment of enzymes or indeed any other bioactive agent and as such may form the basis of the fabrication of a wide range of biosensors. Finally, since the platform used is based on lithographically-deposited gold electrodes on silicon, we note that it is also very suitable for further miniaturisation, mass production and packaging- all of which would serve to reduce production costs.

Received 28th August 2019,
Accepted 11th November 2019

DOI: 10.1039/c9an01664c

rsc.li/analyst

Introduction

Electrochemical biosensors recognize the corresponding analyte through a catalytic or binding event occurring at the surface of the electrode and as a result of the high-sensitivities that have been achieved they have been extensively studied in various clinical, environmental, industrial and agricultural applications.[1–3] The close relationship between analytical performance and the characteristics of the electrode has stimulated considerable efforts devoted to the design and fabrication of miniaturised electrodes. Silicon-based microfabricated electrodes, in particular those based on lithography, etching and deposition show considerable promise for the relatively low-cost batch fabrication of a range of highly-reproducible microelectrodes or arrays of microelectrodes whose precise dimensions and shapes may be directly controlled *via* the choice of a suitable mask.[4,5] Microelectrodes are commonly used for electrochemical analysis[6,7] and biosensing[4] due to several well-established advantages of such electrodes including small size, fast response time, high signal-to-noise ratio and the rapid generation of a steady state response.[6,8,9]

In our previous work we demonstrated how the combination of microfabricated electrodes with nanostructured overlayers can be used most effectively for the sensitive, rapid and reliable detection of glucose *via* both enzymatic and non-enzymatic electrochemical processes.[4,5,10] In those studies the advantages of increased active surface area achieved *via* either metal nanoparticle (Au) attachment or metal (Cu) foam electrodeposition was clearly demonstrated. Especially, the use of the metal foams for the creation of a high active surface area sensor is a particularly attractive approach since such foams may be readily formed *in situ via* an electrodeposition process that utilises the so-called dynamic hydrogen bubble template method.[10–13]

In this present work we continue with this approach, utilising gold foam (Au-foam) electrodeposition onto micro band

[a]Tyndall National Institute, University College Cork, Lee Maltings Complex, Dyke Parade, Cork, Ireland. E-mail: vuslat.buk@tyndall.ie
[b]School of Chemistry, University College Cork, Cork, Ireland

†Electronic supplementary information (ESI) available. See DOI: 10.1039/c9an01664c

array electrodes in acidic solution at high negative overpotentials to form a very elegant, highly porous foam nanocrystal deposit along each single band of the array electrode. We then subsequently modify the Au-foam surface using the electrodeposition of an organic functional layer (OFL) consisting of a chitosan (CS)/carbon nanotube (CNT) composite material. CS was chosen as the major component of the OFL since it possesses excellent characteristics in terms of biocompatibility, nontoxicity, good water permeability low-cost, non-antigenic, abundant functional groups and biodegradability.[14–17] From the point of view of functionalisation, the amine ($-NH_2$) groups present in CS make it a superb candidate for surface modification and the immobilisation of a wide variety of biomolecules. In addition, it is known that combining CS with CNTs not only increases the mechanical stability and robustness of the layer but also greatly enhances its conductivity/rate of electron transfer and electrocatalytic properties.[18–21] After the anodic electrodeposition of the Au-foam and the subsequent cathodic electrodeposition of CS in the presence of the CNTs resulting in the formation of the CNT-embedded composite OFL, the enzymes glucose oxidase and horseradish peroxidase were immobilised onto the functionalised surface by drop casting so as to create a dual-enzyme sensing platform. We show here that the resulting dual-enzyme microbiosensor exhibited a sensitivity of 261.8 μA mM^{-1} cm^{-2} towards glucose detection while also being reproducible (RSD, 3.30%) and relatively unaffected by the common interferences found in human blood serum. These data serve to illustrate the enormous potential that this microfabricated electrode/porous metal/OFL approach possesses in terms of the reliable, reproducible and cheap fabrication of a wide range of sensors.

Materials and methods

Chemicals and instrumentation

Glucose oxidase (EC 1.1.3.4, from Aspergillus niger; GOx), horseradish peroxidase (EC 1.11.1.7; HRP), gold(III) chloride trihydrate ($HAuCl_4{\cdot}3H_2O$), multi-walled carbon nanotube (–COOH), chitosan, glucose, ascorbic acid, uric acid, acetaminophen, acetone, potassium ferrocyanide ($K_4[Fe(CN)_6]$), potassium ferricyanide($K_3[Fe(CN)_6]$), phosphate buffer saline tablets (PBS, 0.01 M, pH 7.4), sterile human serum, potassium chloride (KCl), sulfuric acid (H_2SO_4), sulfuric acid, 1-ethyl-3-(3-dimethylaminopropyl) carbodiimide (EDC), and *N*-hydroxysuccinimide (NHS) were obtained from Sigma-Aldrich. Acetic acid was obtained from Riedel-de Haen. All solutions were prepared with deionized water (18.3 MΩ, ELGAPurelab Ultra).

Scanning electron microscopy (SEM) (Zeiss Supra 40 SEM at accelerating voltages in the range of 5–10 kV) was used to study of the surface morphology of bare and modified band array electrodes. Energy dispersive X-ray analysis (EDX) was performed using a Quanta 650 Field Emission Gun (FEG) attached with an EDX unit, with an accelerating voltage of 20 kV. The chemical composition of the surfaces was studied by using X-ray photoelectron spectroscopy (XPS, Kratos AXIS ULTRA) with Al K_α at 1486.58 eV. The analysis area was approximately 1 mm^2 and the depth of analysis was approximately 10 nm. All the XPS data were calibrated by the carbon 1s peak at 284.8 eV.

Au-Foam/CS–MWCNT/GOx–HRP micro band array biosensor preparation

Gold band array electrodes on silicon were fabricated by a microfabrication process which includes lithography, deposition and etching as we reported earlier.[4,5,10] Firstly the thermal growth of an oxide layer on the silicon substrate was achieved after a series of cleaning steps of the substrate and treated with argon plasma. This was followed by the spin-coating process of a photoresist layer. Then metal deposition of titanium and gold was applied by using e-beam evaporation and wafer was patterned by using a lift off procedure. Silicon nitride with 200 nm thickness was deposited by plasma-enhanced chemical vapour deposition and the mask designed for band array was applied by passivation lithography and etching to obtain electroactive surface areas of the band electrodes on the array and connection pad. Finally, the wafer was covered by a resist layer to protect electrodes during the dicing process. The microfabricated band array electrode has a 200 nm recess depth which is the thickness of the Si_3N_4 passivation layer on the silicon wafer. A typical system consisted of three individual gold band electrodes of length 2000 μm and width 40 μm. Prior to the use of the electrodes, they were cleaned with organic solvents and a plasma cleaner to remove the resist as we have described in detail previously.[4,5,10] All electrochemical measurements were performed on an Autolab workstation (Metrohm, UK) at room temperature. The electrochemical setup consisted of a micro band array electrode as a working electrode, a spiral Pt wire electrode as a counter electrode and an Ag/AgCl (1 M KCl) electrode as reference electrode. Electrodeposition of Au-foam was carried out by applying a chronoamperometric method in a solution of 1.2 mM $HAuCl_4{\cdot}3H_2O/H_2SO_4$ (2.4 M) at a potential of −7 V for 60 seconds. The Au-foam electrodes prepared were covered with a layer of CS–MWCNT nanocomposite by applying another chronoamperometric deposition process in which a potential of −3 V was applied for 25 seconds in 2 mL electrolyte consisting MWCNT and CS. To prepare the stock solution of the CS–MWCNT, 0.1 g CS was solved in 20 mL of 0.1 M acetic acid solution and mixed overnight. Then 5.2 mg MWCNT was added into CS solution and kept in ultrasonicator until to obtain a homogeneous distribution of MWCNTs. 200 μL of the deposition solution of CS–MWCNT was added into 1800 μL double distilled water and used immediately for CS–MWCNT layer deposition. Following completion of this process the electrodes were washed with double distilled water and dried at room temperature. Scheme 1 illustrates the 2-step electrodeposition process used to fabricate the Au-foam/CS–MWCNT band array electrode. After the matrix preparation by the electrochemical approaches, the GOx–HRP enzyme mixture was immobilised onto the surface. For this purpose, an immobilisation solution was prepared which contained 0.16U GOx and

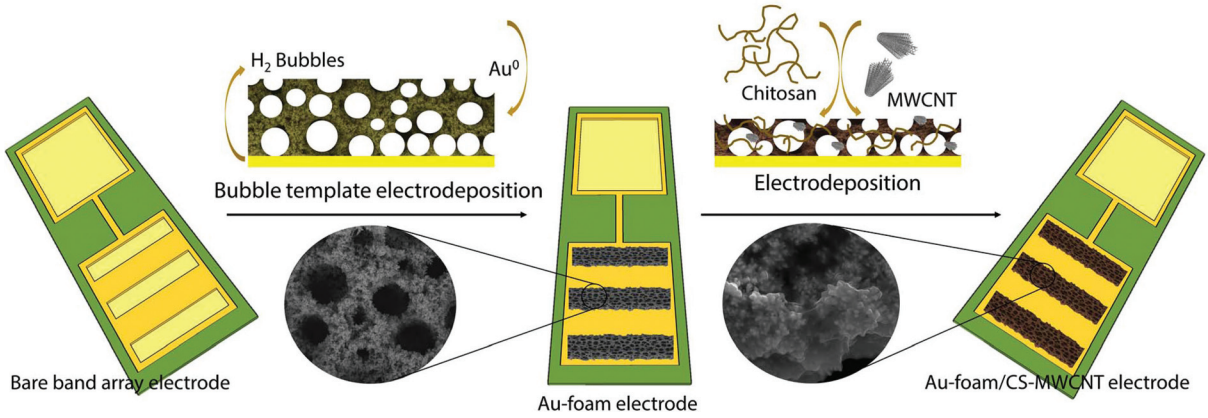

Scheme 1 Illustration of the 2-step electrochemical deposition process used to fabricate the Au-foam/CS–MWCNT electrode.

8U HRP, mixed with 2 μL of NHS/EDC (molar ratio of 1 : 4). The immobilization mixture was drop-cast onto the surface and the electrodes were kept in the fridge at +4 °C for overnight. Finally, the electrodes were washed gently to remove the unbound enzyme molecules and stored in the fridge when not in use. Cyclic voltammetry was applied to investigate the changes of the surface characteristics after each electrodeposition and modification step in a solution of 5 mM $Fe(CN)_6^{3-/4-}$ as a redox probe containing 0.1 M KCl, 0.01 M PBS (pH 7.4).

Results and discussion

Micro band array electrode characterisation

Micro band array electrodes consisting of three gold band individual electrodes with 40 μm width, 2000 μm length were designed and fabricated by standard lithography. Fig. 1A and B and inset show the SEM images of the bare band array electrodes after the fabrication process at both low and high magnification. As can be seen in Fig. 1A, the SEM micrograph shows the three well-arranged individual band electrodes of length 2000 μm on the insulation layer with an 800 μm inter-electrode-distance between them. Fig. 1B shows a higher magnification image of the end of one of the electrodes which clearly displays the well-defined shape of the band electrode of width 40 μm. An SEM image of the edge of the corner of a single band electrode is then displayed in Fig. 1B-inset where the higher magnification clearly shows the ability of the microfabrication process to produce highly smooth gold surfaces.[4] Fig. 1C is a schematic representation of the whole electrode showing the three band array electrodes, the connection track and the connection pad. The elemental composition of the gold surface and the passivated surface were studied using EDX. The SEM-EDX spectral analysis results are shown in Fig. S1 (ESI†). The elements of Au (83.9%), Si (15.3%) and Ti (0.7%) were detected on the electrode active surface area (Fig. S1A, ESI†), where the silicon was the substrate material and the titanium was used as an adhesion layer. On the passivation area, Si (63.4%), O (20.3%, presumably from the atmosphere) and N (16.2%) were detected, indicating the silicon nitride (Si_3N_4) passivation layer Fig. S1B (ESI†). These results indicate the success of the microfabrication steps including deposition, lithography and etching. Cyclic voltammetry (CV) was used to study the characteristics of the bare micro band array electrodes. Fig. 1D shows cyclic voltammograms recorded from the three individual band array electrodes in a solution of 5 mM $Fe(CN)_6^{3-/4-}$ as a redox probe in 0.01 M PBS (pH 7.4), containing 0.1 M KCl. As shown in the Fig. 1D, the micro band array electrodes all exhibit highly reproducible voltammograms. However, the designed electrode tended towards slightly peak-shaped voltammogram presumably due to the partially overlapping or close diffusion hemispheres of each band on the array. The voltammetry is intermediate between the diffusionally independent profile (category 2) and linear diffusion (category 4).[22] The effect of scan rate on the voltammetric response was also investigated, Fig. S2.† At high scan rate a peak-shaped voltammogram was observed due to the increased contribution from linear diffusion profile, Fig. S2 (inset).†

Au-Foam and CS–MWCNT electrodeposition, characterisation and the construction of the biosensor

SEM was used to explore the morphological characteristics of the electrodeposits of Au foam and the CS–MWCNT composite. Fig. 2A presents an image of the Au foam band array electrode. As can be seen, a highly homogenous distribution of Au foam was achieved as a result of the controlled electrodeposition process. Fig. 2B shows an SEM image of a small portion of a single band electrode at higher magnification. From these images it is clear that the Au foam deposits are three-dimensional and highly porous (Fig. 2C). Fig. 2D demonstrates the nanostructured nature of the gold foam wall.

After the electrodeposition of the gold foam, the wall of the foam was covered by a thin film of the chitosan gel by applying −3 V for 25 seconds in the presence of MWCNTs. This process results in the formation of an insoluble chitosan layer on the surface due to the pH changes that occur near to the electrode surface. Furthermore, while the chitosan monomers are accumulating at the electrode surface, the MWCNTs may

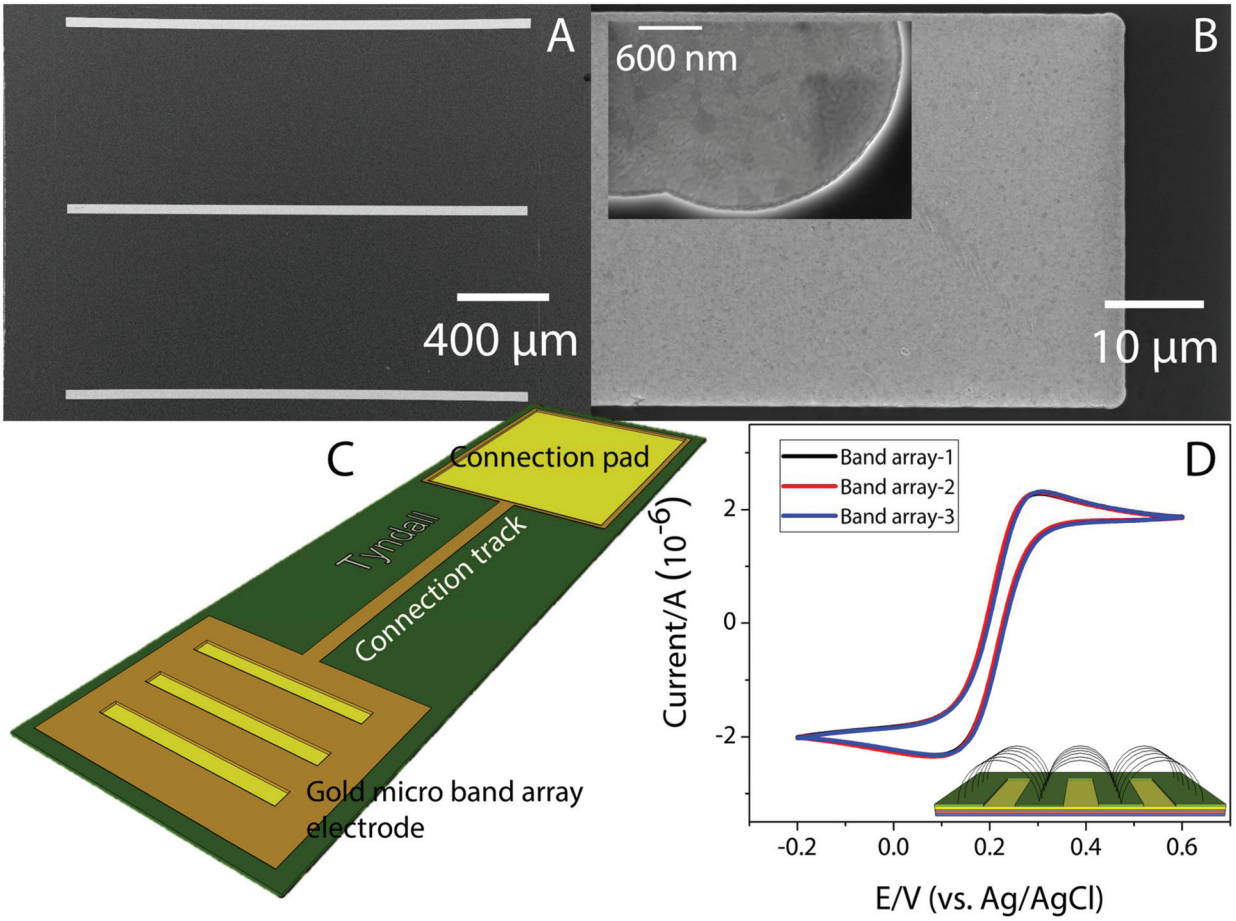

Fig. 1 SEM images of the bare micro band array electrode; (A) all three bands (low magnification), (B) the edge of the single band electrode (INSET: single band electrode corner-high magnification); (C) schematic illustration of microfabricated band array electrode; (D) overlay cyclic voltammograms of individual three band array electrodes at a scan rate of 5 mV s^{-1} in a solution of 5 mM $Fe(CN)_6^{3-/4-}$ as a redox probe in 0.01 M PBS (pH 7.4), containing 0.1 M KCl and the associated diffusion zones.

become trapped in the thin film of chitosan gel as it forms. Fig. 2E shows the whole array electrode after CS–MWCNT electrodeposition. The changes in contrast that are seen following CS–MWCNT electrodeposition are due to the addition of this organic functional layer (OFL) with a darker appearance being associated to a thicker OFL. As it can be seen in Fig. 2F, the OFL encapsulates the walls of the gold foam. This is more apparent from the higher magnification images presented in Fig. 2G and H. Following the drop casting of the enzymes onto the electrode, the effect of the electrodeposition time and hence thickness of the OFL on the current responses of the completed biosensor was studied, Fig. S3A (ESI†). From this figure it may be seen that the optimum current value was obtained for an electrode prepared using 25 seconds deposition time to deposit the OFL. Lower deposition times (20 seconds) showed a decreased current level which we suggest may be due to insufficient amounts of the polymer deposits which in turn results in an insufficient number of the functional groups used to attach the enzyme molecules onto surface, leading to a reduction in the amount of immobilised enzymes. However, the figure also reveals that higher deposition times for the OFL also resulted in a decrease in the current response of the sensor. We suggest that this may be due to the presence of a thicker, polymeric OFL which may act as an insulation layer due to the poor conductivity of the polymer. In addition, over deposition of the OFL may lead the formation of a more compact film which may hinder electron transfer and solution diffusion.[23,24] Thus it is apparent that the thickness of the particular OFL used in this study is a factor which requires some optimisation.

The electrodeposited materials were studied further using XPS and EDX. Fig. 3 displays the spectra obtained for each analysis. The XPS survey spectrum (Fig. 3A) confirms the presence of Au, O and C (mostly from atmosphere). Fig. 3B shows the high resolution Au 4f XPS spectra of the Au-foam. The Au $4f_{7/2}$ and Au $4f_{5/2}$ peaks were centred at 85.0 and 88.7 eV binding energy, respectively, which indicate the presence of metallic gold. The spectrum also shows a peak at ~84.0 eV ($4f_{7/2}$). This peak is also believed to arise from the bulk gold where the observed shift in energy may be attributed to possible size-related changes in the electronic structure of the material resulting from its nanostructured nature, to the possible pres-

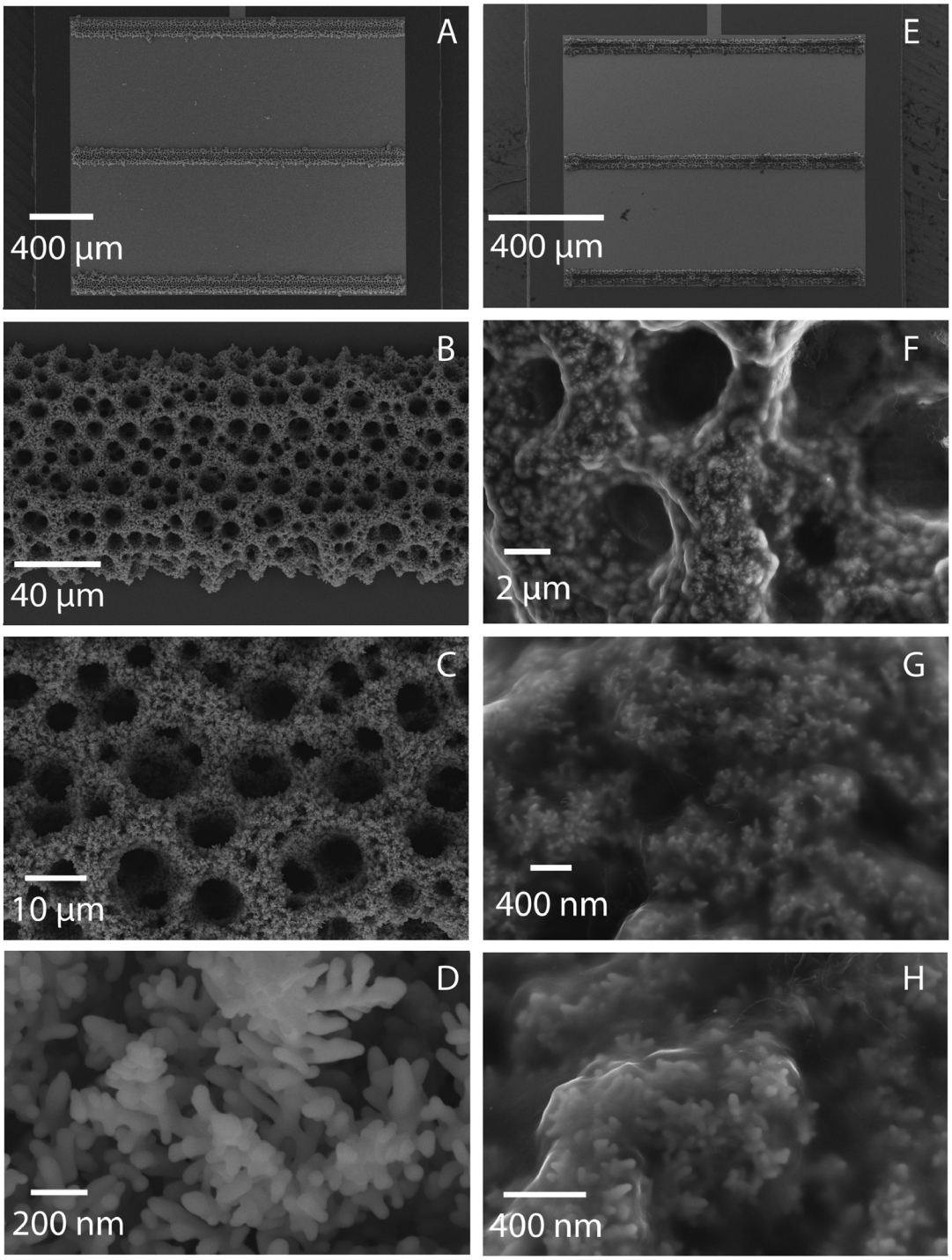

Fig. 2 SEM images of (A) the Au-foam deposited band array electrode, (B) an Au-foam single band electrode, (C) showing the pore structure of the deposits, (D) showing nanocrystals of the Au-foam wall at higher magnification, (E) the Au-foam band array after CS–MWCNT electrodeposition, (F) the Au-foam/CS–MWCNT pores, and (G and H) SEM images of the CS–MWCNT nanocomposite film electrodeposited nanocrystals with higher magnification.

ence of oxides or to the influence of the underlying support materials ($Au/TiO_2/SiO_2/Si$) and treatment conditions.[25,26] However, the Au 4f doublet peaks are sufficiently narrow, with a FWHM of 0.68 eV, to be a good indicator of metallic Au. The 'peaks' at 88.2 and 89.4 eV binding energies which are suggested by the line fitting analysis as shown are possibly related to the presence of Au(III) and similarly the peak at 85.8 eV binding energy may be related to a species that is labelled as $Au^{\delta+}$, which is essentially non-metallic gold but not in the +3 oxidation state. It is suggested that these weaker

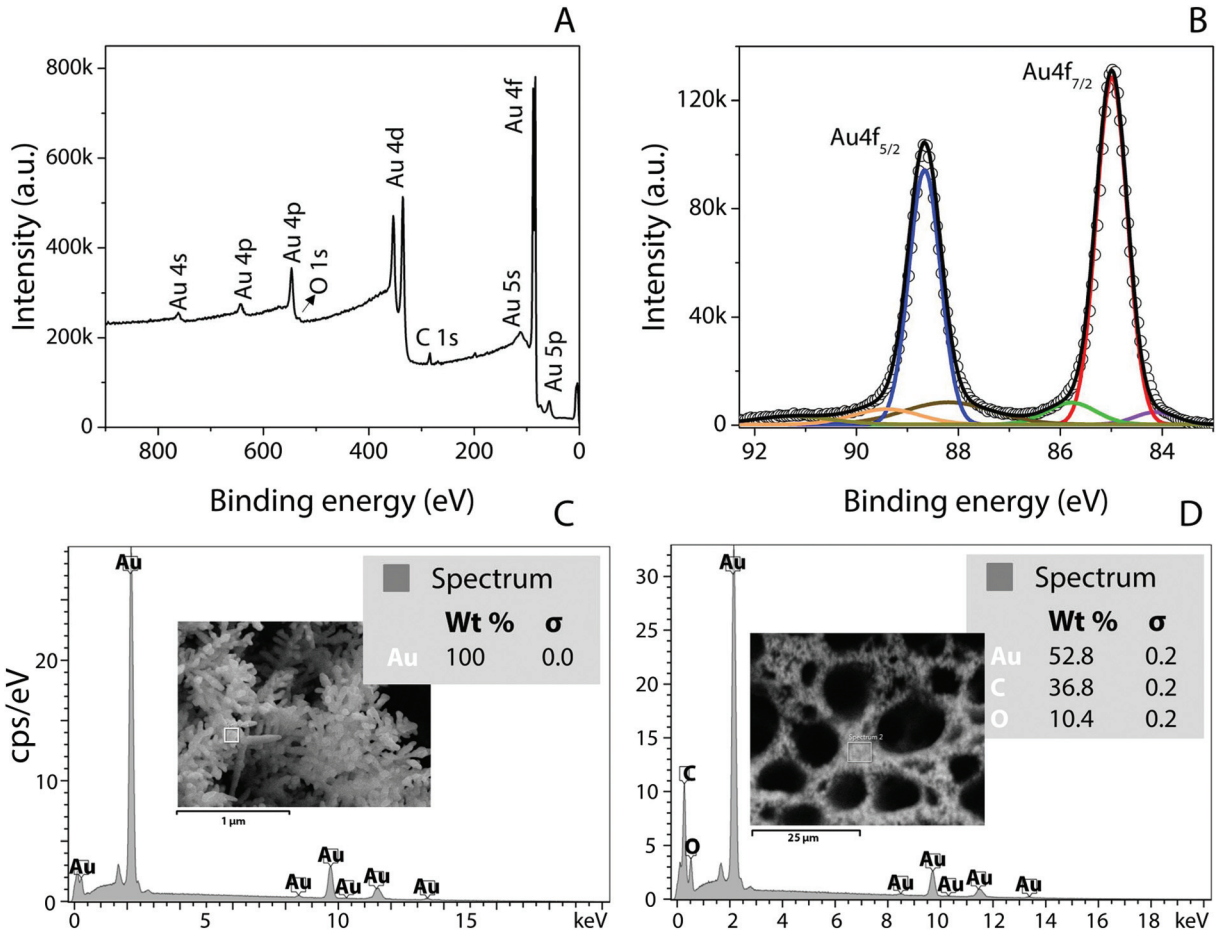

Fig. 3 (A) An XPS survey spectrum of the Au-foam, (B) a high resolution XPS spectrum of the Au 4f region, (C) an EDX spectrum recorded from the Au-foam and (D) an EDX spectrum recorded from the Au-foam/CS–MWCNT.

features most likely result from the presence of some oxide material.[27]

EDX also reveals the presence of the gold, as expected, Fig. 3C. In addition, EDX reveals that following electrodeposition of the OFL the elemental composition of the material changes, also as expected, Fig. 3D. From Fig. 3D it can be seen that following deposition of the OFL the surface is composed of Au (52.8%), C (36.8%) and O (10.4%).

The ratio of enzyme loading onto Au-foam/CS–MWCNT surface was also studied, Fig. S3B (ESI†). A series of different molar ratios of GOx : HRP (0.01, 0.015, 0.02 and 0.025) were immobilised onto the Au-foam/CS–MWCNT OFL band array electrode surface. As may be seen from this figure a molar ratio of 0.02 GOx to HRP exhibited the maximum biosensor response. At lower ratios a gradual decrease in current is observed due to the decreasing concentration of the GOx enzyme on the surface. However, a decrease in current is also observed at higher ratios. Although these are preliminary data we may suggest that it is not unreasonable to expect there to be an optimum ratio for the operation of the dual enzyme mechanism based on orientation and conformation factors for the immobilised species and the ease with which the glucose may approach the active sites on the enzymes.[23] As a result of this study a molar ratio, GOx : HRP of 0.02 was adopted in the development of the biosensor.

Fig. 4A shows typical cyclic voltammograms recorded from the bare gold band array electrodes and gold foam deposited array electrodes in 0.5 M H_2SO_4. Both surfaces showed a similar electrochemical response, but the current values recorded are very different, with the current observed from the foam electrode being much larger. The foam structured metals are very well-known to be highly porous, possessing very large surface areas. Thus, it is to be expected that in comparison with the bare gold band electrodes the Au foam electrodes would show a much higher response, as shown. Fig. 4B represents the voltammograms recorded after the various surface modifications. Clearly, the very large active surface area of the Au-foam deposits resulted in a significant increase in the peak current in comparison to that observed for the bare band array electrode. However, Fig. 4B also reveals that following the electrodeposition of the Au foam the shape of the voltammogram changes, adopting the typical shape associated with a voltammogram which arises from a mixture of both planar and radial diffusion. This is most likely due to the increased width of

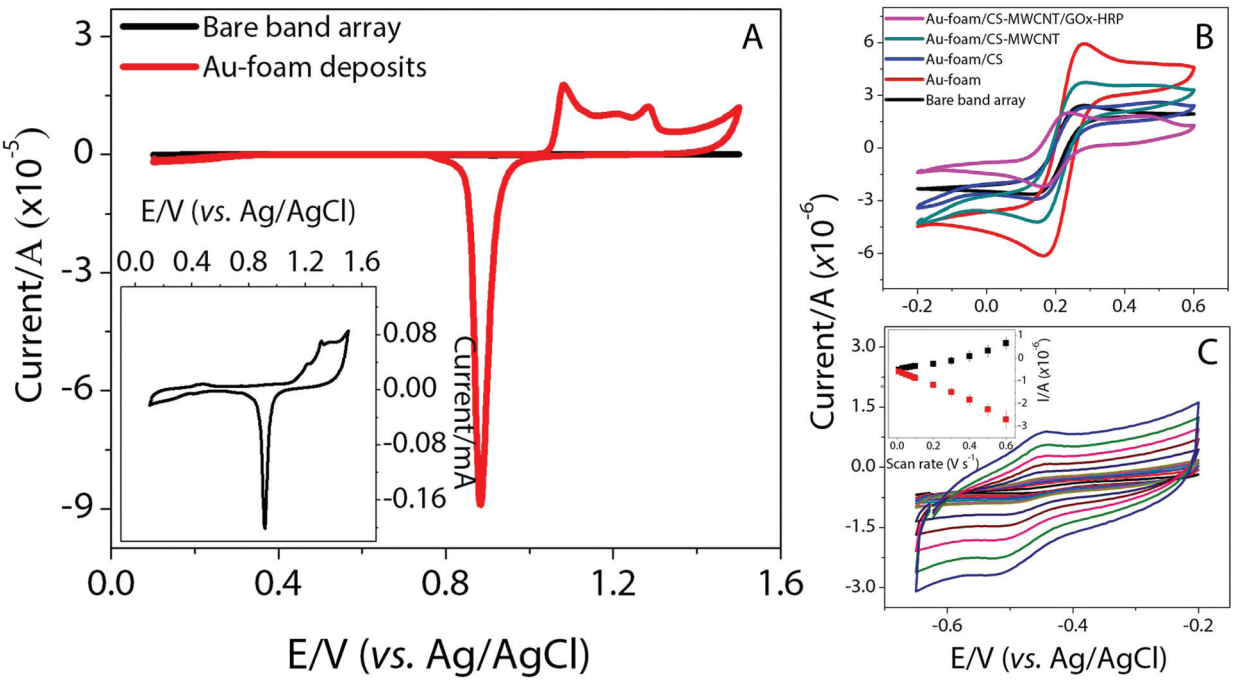

Fig. 4 (A) CVs recorded from the bare and Au-foam deposited band array electrodes in in 0.5 M H_2SO_4, (B) CVs recorded from the bare, Au-foam, Au-foam/CS, Au-foam/CS–MWCNT and Au-foam/CS–MWCNT/GOx–HRP modified band array electrodes in 5 mM $Fe(CN)_6^{3-/4-}$ as a redox probe containing 0.1 M KCl, 0.01 M PBS (pH 7.4), (C) CVs recorded from the complete biosensor at the scan rates of 0.01, 0.03, 0.05, 0.07, 0.09, 0.1, 0.2, 0.3, 0.4, 0.5, 0.6, 0.7 V s^{-1} in 0.01 M PBS (pH 7.4).

each band of the array after deposition of foam structures, which may cause overlapping diffusion zones to arise between the adjacent Au-foam band electrodes. It might be expected that if we cover a conductive surface like the Au/Au foam with a non-conductive polymer that a decrease in the peak current of the electrode should result. However, we find that the presence of the MWCNTs appears to improve the conductivity of the OFL resulting in higher current. Moreover, the immobilisation of the enzymes on the surface results in a decrease of the peak current due to the blocking action of the enzymes towards the test redox couple, as can be seen in Fig. 4B.

The effect of the scan rate on the voltammetric response was also studied in 0.01 M PBS (pH 7.4). High scan rates lead a decrease in the size of diffusion layer which causes the appearance of increased current levels. As shown in Fig. 4C, both anodic and cathodic peak currents increase linearly with increased scan rates from 0.01 to 0.7 V s^{-1}, suggesting a surface-controlled process.[28,29]

The GOx–HRP dual enzyme system is a cascade scheme where HRP is catalytically linked to GOx, may provide several advantages including signal amplification of the biosensor response and decreased peroxide-induced degradation of immobilised GOx as a result of removal of H_2O_2.[30] Such systems were developed for glucose detection commonly in the presence of an oxidized mediator for the regeneration of the oxidase.[31–33] Here, we have developed a dual-enzyme system without redox mediators. Fig. 5A exhibits the CVs obtained from a dual enzyme electrode (i: Au-foam/CS–MWCNT/GOx–HRP) and a single enzyme electrode (ii: Au-foam/CS–MWCNT/GOx) in the absence and presence of glucose in PBS. A weak reduction peak was observed at the Au-foam/CS–MWCNT/GOx biosensor in the absence of glucose and a decrease of the reduction peak current after glucose addition due to the consumption of the dissolved oxygen by the following enzyme catalyzed reactions (1) and (2);[5,34,35]

$$\mathrm{GOx(FAD)} + \mathrm{glucose} \rightarrow \mathrm{GOx(FADH_2)} + \mathrm{Gluconic\ acid} \quad (1)$$

$$\mathrm{GOx(FADH_2)} + \mathrm{O_2} \rightarrow \mathrm{GOx\ (FAD)} + \mathrm{H_2O_2} \quad (2)$$

However, the Au-foam/CS–MWCNT/GOx–HRP biosensor showed greater response towards glucose at −0.45 V without any redox mediator in comparison to single enzyme sensor (Fig. 5i). This reflects the great cascade scheme of the developed biosensor which is based on the current decrease of the dissolved oxygen. The mechanism can be explained as below. HRP contains the heme as a prosthetic group, which is also the active site of the protein (with resting state of the heme-iron: Fe(III)). HRP reacts with H_2O_2 to form compound I which is a two-equivalent oxidized form containing oxyferryl heme (Fe^{4+} = O) and H_2O (eqn (3)).[34] In turn, compound I is further reduced (eqn (4)) or it also may produce HRP(Fe^{3+}), O_2 and H_2O if it reacts with the H_2O_2 as proton and electron donor (eqn (5)).[36–38]

$$\mathrm{HRP(Fe^{3+})} + \mathrm{H_2O_2} \rightarrow \mathrm{Compound\ I\ [HRP(Fe^{4+} = O)]} + \mathrm{H_2O} \quad (3)$$

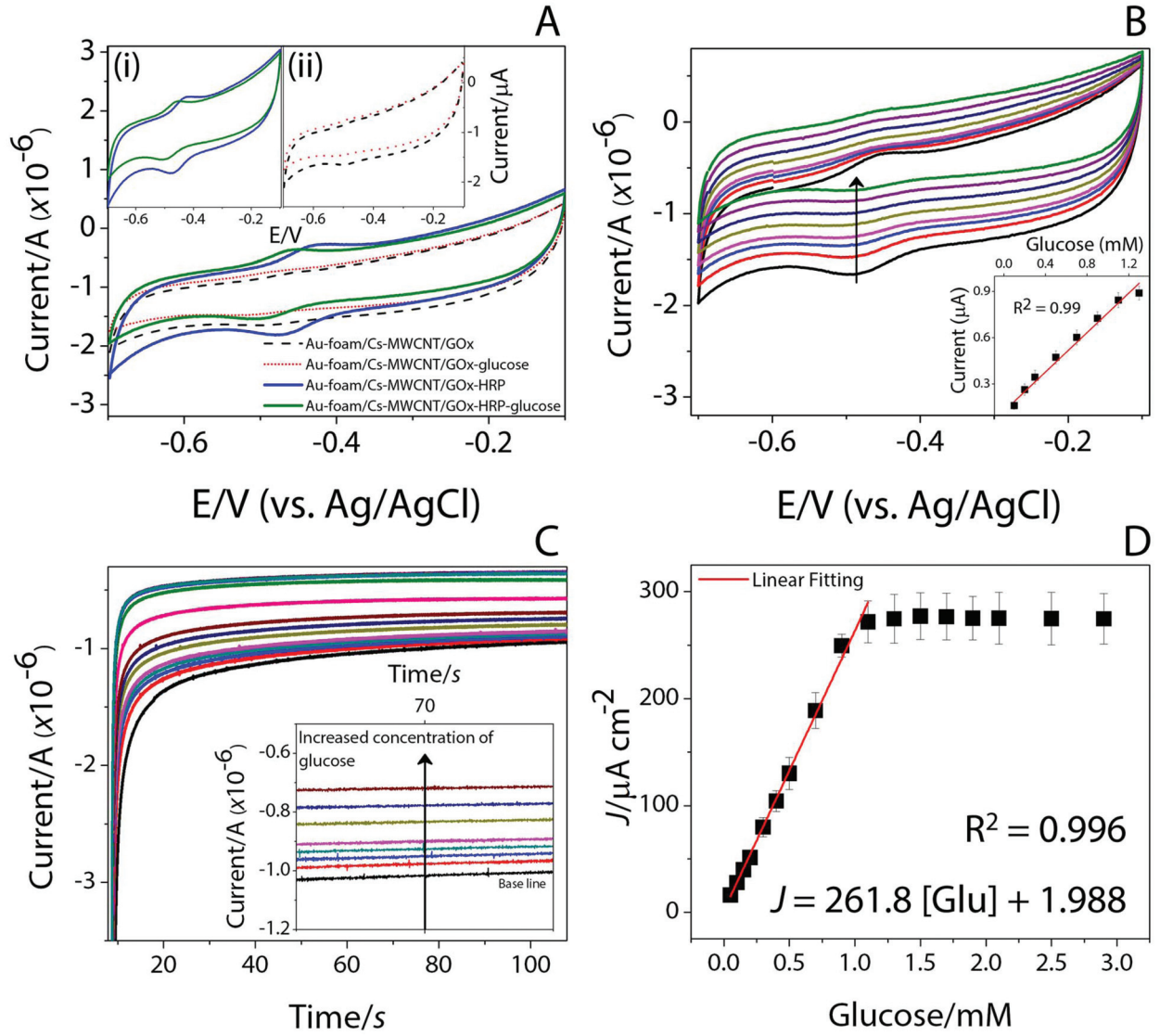

Fig. 5 (A) CVs recorded from Au-foam/CS–MWCNT/GOx and Au-foam/CS–MWCNT/GOx–HRP modified band array electrodes in the absence of presence of 0.1 mM glucose in 0.01 M PBS (pH 7.4) at a scan rate of 0.05 V s^{-1} (inset; individual graphs of (i)Au-foam/CS–MWCNT/GOx–HRP and (ii) Au-foam/CS–MWCNT/GOx (B) CVs recorded from the Au-foam/CS–MWCNT/GOx–HRP microbiosensor with increasing concentrations of glucose in 0.01 M PBS (pH 7.4) (inset: corresponding linear range), (C) the chronoamperometric response of the biosensor towards glucose with increasing concentration of glucose at a applied potential of −0.45 V (inset: the magnified graph of 60th second of amperograms of the base and first seven additions), and (D) the corresponding calibration curve obtained from the amperograms recorded from the biosensor.

$$\text{Compound I } [\text{HRP}(\text{Fe}^{4+}=\text{O})] + 2\text{e}^- + 2\text{H}^+ \rightarrow \text{HRP}(\text{Fe}^{3+}) + \text{H}_2\text{O} \quad (4)$$

$$\text{Compound I } [\text{HRP}(\text{Fe}^{4+}=\text{O})] + \text{H}_2\text{O}_2 \rightarrow \text{HRP}(\text{Fe}^{3+}) + \text{O}_2 + \text{H}_2\text{O} \quad (5)$$

Furthermore the biosensor was studied by applying cyclic voltammetry in a series of standard glucose solutions in 0.01 M PBS (pH 7.4). Fig. 5B shows the corresponding CVs recorded after each addition of glucose into electrochemical cell. With increasing concentration of glucose, a decrease of the reduction current and an increase of the oxidation current is observed due to the consecutive catalytic reactions induced by both enzymes with firstly the glucose and secondly the hydrogen peroxide. The inset graphs (Fig. 5B) demonstrate the linear relationship between the glucose concentration and the reduction current density with a correlation coefficient (R^2) of 0.99. This result reveals that the dual-enzyme biosensor developed has some considerable potential for the detection of glucose *via* these enzymatic processes.

Chronoamperometric detection of glucose by Au-foam/CS–MWCNT/GOx–HRP micro band array biosensor

Fig. 5C displays the chronoamperograms obtained by using the Au-foam/CS–MWCNT/GOx–HRP micro band array bio-

Table 1 The analytical performance comparison list of dual-enzyme biosensors available in literature

	Sensitivity	Linear range	Detection limit	Reproducibility	Reusability, repeatability, or operational stability	Long term stability	Ref.
Polymerized-multiporous SnO_2 nanofibers/HRP/GOx	—	5–100 μM	1.8 μM	—	3.5% (RSD), n = 10	94%, after 60 days	39
Au/SWNT/GOD–HRP/PPy	7.01 ± 0.18 μA mM^{-1} cm^{-2}	0.030–2.43 mM	0.03 ± 0.009 mM	5.4% (RSD), n = 8	A decrease of 35% within 10 h, good operational stability	82% and 67% of after 1 and 2 weeks	40
Au/MPS/TH/$(SCGNPs/TH)_6$/GOx/HRP	3.8 μA mM^{-1} cm^{-2}	up to at least 3.0 mM	3.5×10^{-5} M	—	—	80%, 3 weeks	41
GC/[TMOS–HRP–graphite]–[TMOS–GOD]	2.95 mA M^{-1} cm^{-2}	Up to 0.70 mM	—	—	—	74%, one week	42
(GOD/PPy) membrane on the surface of (FCA)-mediated (HRP)-modified CCE	1.11 μA mM^{-1}	8.0×10^{-5}–1.3×10^{-3} M	1.0×10^{-5} M	—	—	68%, 3 weeks	43
GC/CNT/GOx + HRP/PTBO	113 mA M^{-1} cm^{-2}	0.1–1.2 mM	0.03 mM	4.3% (RSD), n = 8	—	75%, 25 days	44
fMWCNT–TB–GOx–HRP–Nf	8.3 μA mM^{-1} cm^{-2}	1.5×10^{-8}–1.8×10^{-3} M	3×10^{-9} M	2.5%(RSD), n = 10	1.9% (RSD), n = 8	95%, 4 months	45
GOD–HRP–Cys–SG/GNP/ITO	131.7 nA $mmol^{-1}$ L^{-1}	0.02–3.2 mmol L^{-1}	0.01 mmol L^{-1}	6.7%(RSD), n = 5	3.1%(RSD), n = 9	80%, 2 months	30
GOx–CS–HRP/AgNCs–CS	—	10 μM–1.5 mM	0.6977 μM	1.27%(RSD), n = 6	2.14%(RSD), n = 4	93%, 9 days; 70%, 2 weeks	46
Nf–GOD–HRP/Au–Fe_3O_4@SiO_2/ITO	(1) 92.14, (2) 15.00 μA mM^{-1} cm^{-2}	(1) 0.05–1.0 mM, (2) 1.0–8.0 mM	0.01 mM	5.2% (RSD), n = 6	3.7% (RSD), n = 5	97.2%, 25 days; 94.8%, 30 days; 50% 60 days	47
HRP–GOD/Con A/CS	1.18 μA mM^{-1}	1.0×10^{-6}–2.2×10^{-4} M	6.7×10^{-7} M	3.8%(RSD), n = 6	2.9% (RSD), n = 7	89%, 5 weeks	48
PANI|HRP–GOD|MWNTs	0.94 μA mM^{-1}	0.05–12 mM	0.02 mM	9.5%(RSD), n = 8	—	—	49
MWNT/TH/GOD/HRP/Nf	—	10 nM–10 mM	3 nM	—	2.3% (RSD), n = 9	>90%, 90 days	50
Au-Foam/CS–MWCNT/GOx–HRP micro band array biosensor	261.8 μA mM^{-1} cm^{-2}	0.05–1.3 mM	25 μM	3.30% (RSD), n = 7	4.41%, 3.93% and 4.99% (RSD), n = 10 for each biosensor	No significant change after 45 days	This study

Abbreviations: Au: gold, SWNT: single-walled carbon nanotube, Ppy: electropolymerized pyrrole, MPS: 3-mercapto-1-propanesulfonic acid sodium salt, SCGNPs: sulfonate-capped gold nanoparticles, TH: thionine, TMOS: Tetramethoxysilane, GC: glassy carbon electrode, FCA: Ferrocenecarboxylic acid, CCE: sol–gel derived composite carbon electrode, PTBO: poly(toluidine blue O), CNT: Carbon nanotube, fMWCNT: functionalized multiwalled carbon nanotubes, TB: Toluidine blue, Nf: Nafion, Cys: Cysteine, SG: silica sol–gel, GNP: gold nanoparticles, ITO: indium tin oxide, AgNCs: Silver nanocubes, CS: Chitosan, Con A: Concanavalin A, PANI: polyaniline, MWCNTs: multiwalled carbon nanotubes.

sensor at an applied potential of −0.45 V. The inset graph (Fig. 5C) shows the 70th second of amperograms belong to the base line and first 7 subsequent additions of glucose. Fig. 5D demonstrates the corresponding calibration curve of the biosensor, obtained by subtraction of the current values at 70th second from the base line current value at the same second. As it can be seen in the Fig. 5C and the inset, each amperogram reaches steady-state current level very quickly, which is one of the most important advantages of the miniaturised systems that form the basis of our work.[4,10] The biosensor developed exhibited a linear range from 0.05 mM to 1.1 mM with the linear regression equation of J (μA cm^{-2}) = 261.8 [Glu] (mM) + 1.988 (R^2 = 0.996). The sensitivity of the biosensor was calculated to be 261.8 μA mM^{-1} cm^{-2}. This high value of sensitivity may be attributed to the advantages of the electrode/OFL matrix developed for enzyme immobilisation, being a combination of the gold foam-chitosan–multi walled carbon nanotubes, the use of a dual-enzyme system and the use of micron-scale, band array electrodes. The limit of detection (LOD) was calculated to be 0.025 mM by using the formula, $3s_b/S$ (s_b, standard deviation of the blank; S, sensitivity). A performance comparison of the biosensor developed with the other dual-enzyme biosensors described in the literature is given in Table 1.

Interference effects, stability and reproducibility

To evaluate the selectivity of the biosensor towards glucose in the presence of the common interfering species, three individual biosensors were prepared and studied with glucose, ascorbic acid, acetaminophen and uric acid. Fig. S4 (ESI†) shows chronoamperograms recorded after each addition of the interfering species. Briefly, the prepared biosensors were studied with blank PBS (0.01 M, pH 7.4), and then a 0.4 mM glucose solution was measured. This was followed by the serial additions of 0.1 mM ascorbic acid, acetaminophen and uric acid, respectively. 0.4 mM glucose was studied at the end in the presence of those interfering molecules. Fig. 6A shows a comparison of current densities obtained from the first (glu) and last (glu_{int}) glucose measurements. The calculated changes of the biosensor responses are 11.45%, 10.75% and 9.89%. The operational stability of the developed biosensor was studied by 10 subsequent chronoamperometric measurements of three individual biosensors. Fig. 6B displays the current densities obtained from each experiment, for each biosensor. The calculated standard deviations for each biosensor in regard to operational stability are 4.41%, 3.93% and 4.99%. After storing the biosensor in 0.01 M PBS (pH 7.4) at +4 °C for 45 days, there was no significant change of the response of the biosensor. Seven individual biosensors were prepared and their responses to glucose in 0.01 M PBS (pH 7.4) were measured under the same conditions in order to evaluate the biosensor reproducibility, Fig. 6C. The relative standard deviation towards glucose detection was determined to be 3.30%.

These noteworthy performance results obtained for the biosensor developed indicate the success of the biosensor as an analytical device. While the band array electrode provides a micro-scaled environment, the Au-foam deposit offers a highly porous 3D surface which was optimised to the borders of each band of the array. After the one step electrochemical deposition of chitosan-multiwalled carbon nanotube nanocomposite OFL, the overall matrix becomes a biocompatible microenvironment for biomolecule immobilisation which contributes to maintaining and improving the catalytic activity of the attached enzymes. Furthermore, the developed matrix is highly suitable for high concentration biomolecule immobilisation due to its high surface area.

A real-world application

To demonstrate a possible real world application of our biosensor, sterile human serum samples were used. A sterile serum sample was diluted to 1 : 10 in 0.01 M PBS (pH 7.4) and spiked with two different concentrations of glucose to obtain 0.5 mM and 1 mM glucose concentrations in the electrochemical cell. The biosensor was used to determine the glucose level in both spiked samples, respectively. Firstly, prepared electrodes were studied with chronoamperometry in 0.01 M PBS (pH 7.4) to be used as a baseline. Then spiked serum samples were added into electrochemical cell using the standard addition method, mixed very well and measured by applying chronoamperometry at – 0.45 V. The obtained value

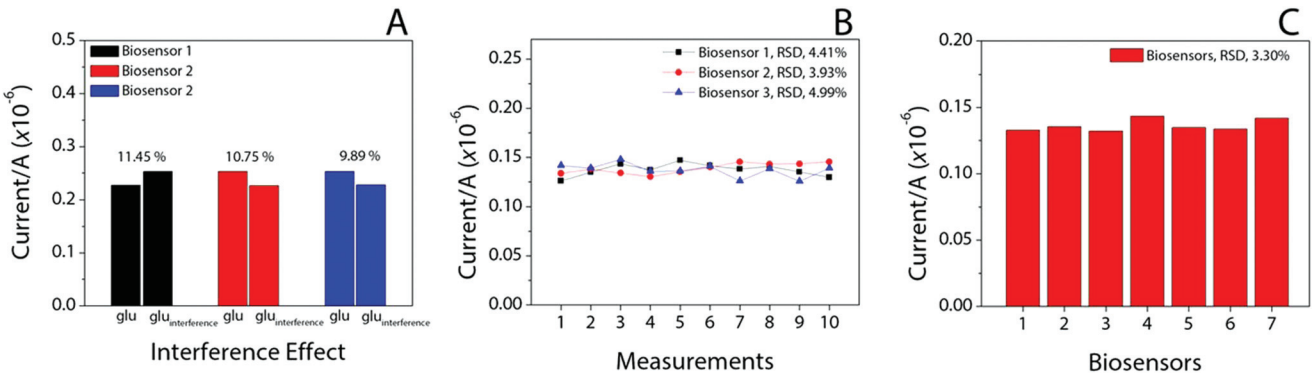

Fig. 6 (A) Interference effects recorded for three individual biosensors, (B) the operational stability of the three individual biosensors, and (C) the reproducibility of the biosensor (n = 7).

Table 2 Determination of glucose in sterile serum samples

Sample	Spiked serum glucose concentration (mM)	Au-Foam/CS–MWCNT/GOx–HRP micro band array biosensor measured glucose concentration	Recovery (%)
1	0.5	0.54 (±0.01)	108
2	1	0.99 (±0.01)	99

at 70th second from spiked serum was subtracted from the baseline value obtained at 70th second to determine the concentration from the calibration curve equation. The results obtained for both spiked samples are shown in Table 2. The obtained concentration of non-spiked sterile serum in the electrochemical cell (0.002 mM < LOD) is neglected due to the lower value than the limit of detection of the developed biosensor.

Conclusions

This paper reports the development of a dual-enzyme micro band array biosensor for the detection of glucose. The in-house microfabricated electrode is a silicon-based highly reproducible micro band array electrode consisting of three bands on the array with 40 μm band-width and 2000 μm band-length. The band array electrode is then modified with 3D gold foam by controlled electrodeposition. The gold foam, being a highly porous material, serves to dramatically increase the active surface area. An OFL in the form of an electrodeposited chitosan-multiwalled carbon nanotubes nanocomposite film is then added as the main immobilisation matrix for glucose oxidase and horseradish peroxidase.

The resulting biosensor showed a sensitivity of 261.8 μA mM^{-1} cm^{-2} and reproducibility (RSD 3.30%, n = 7). Furthermore, it demonstrated a lifetime of up to 45 days (stored at +4 °C, in 0.01 M PBS, pH 7.4). The operational stability of the biosensor demonstrates a very good level of reusability with low RSD values of 4.41%, 3.93% and 4.99%. The biosensor showed corresponding values towards the spiked serum samples with 108% and 99% recovery levels.

The principle benefits of the sensing platform developed here arise from a combination of the micro-scaled matrix architecture used combined with the nanoscale deposits and the highly flexible, biocompatible, easily functionalised OFL material. We suggest there that this platform may be highly suitable for the detection of other biomolecules and further miniaturisation and/or packaging.

Conflicts of interest

There are no conflicts of interest to declare.

Acknowledgements

The authors appreciate the financial support from the Department of Agriculture, Food and the Marine, 14F883, Ireland.

References

1 X.-Y. Lang, H.-Y. Fu, C. Hou, G.-F. Han, P. Yang, Y.-B. Liu and Q. Jiang, Nanoporous gold supported cobalt oxide microelectrodes as high-performance electrochemical biosensors, *Nat. Commun.*, 2013, **4**, 2169.
2 J. Wang, Electrochemical glucose biosensors, *Chem. Rev.*, 2008, **108**, 814–825.
3 A. P. F. Turner, Biosensors: Fundamentals and applications – Historic book now open access, *Biosens. Bioelectron.*, 2015, **65**, A1.
4 V. Buk and M. E. Pemble, A highly sensitive glucose biosensor based on a micro disk array electrode design modified with carbon quantum dots and gold nanoparticles, *Electrochim. Acta*, 2019, **298**, 97–105.
5 V. Buk, M. E. Pemble and K. Twomey, Fabrication and evaluation of a carbon quantum dot/gold nanoparticle nanohybrid material integrated onto planar micro gold electrodes for potential bioelectrochemical sensing applications, *Electrochim. Acta*, 2019, **293**, 307–317.
6 I. Streeter, N. Fietkau, J. Del Campo, R. Mas, F. X. Munoz and R. G. Compton, Voltammetry at regular microband electrode arrays: Theory and experiment, *J. Phys. Chem. C*, 2007, **111**, 12058–12066.
7 J. Okuno, K. Maehashi, K. Matsumoto, K. Kerman, Y. Takamura and E. Tamiya, Single-walled carbon nanotube-arrayed microelectrode chip for electrochemical analysis, *Electrochem. Commun.*, 2007, **9**, 13–18.
8 C. X. Ma, N. M. Contento, L. R. Gibson and P. W. Bohn, Redox Cycling in Nanoscale-Recessed Ring-Disk Electrode Arrays for Enhanced Electrochemical Sensitivity, *ACS Nano*, 2013, **7**, 5483–5490.
9 D. Li, C. Lin, C. Batchelor-McAuley, L. Chen and R. G. Compton, Electrochemical measurement of the size of microband electrodes: A theoretical study, *J. Electroanal. Chem.*, 2019, **840**, 279–284.
10 V. B. Juska, A. Walcarius and M. E. Pemble, Cu Nanodendrite Foams on Integrated Band Array Electrodes for the Nonenzymatic Detection of Glucose, *ACS Appl. Nano Mater.*, 2019, **2**, 5878–5889.
11 D. H. Nam, B. J. Taitt and K. S. Choi, Copper-Based Catalytic Anodes To Produce 2,5-Furandicarboxylic Acid, a Biomass-Derived Alternative to Terephthalic Acid, *ACS Catal.*, 2018, **8**, 1197–1206.
12 W. Lu, Y. Sun, H. Dai, P. Ni, S. Jiang, Y. Wang, Z. Li and Z. Li, Direct growth of pod-like Cu_2O nanowire arrays on copper foam: Highly sensitive and efficient nonenzymatic glucose and H_2O_2 biosensor, *Sens. Actuators, B*, 2016, **231**, 860–866.

13 X. Niu, Y. Li, J. Tang, Y. Hu, H. Zhao and M. Lan, Electrochemical sensing interfaces with tunable porosity for nonenzymatic glucose detection: A Cu foam case, *Biosens. Bioelectron.*, 2014, **51**, 22–28.
14 E. Zhang, R. Xing, S. Liu, Y. Qin, K. Li and P. Li, Advances in chitosan-based nanoparticles for oncotherapy, *Carbohydr. Polym.*, 2019, **222**, 115004.
15 R. Shanmuganathan, T. N. J. I. Edison, F. LewisOscar, P. Kumar, S. Shanmugam and A. Pugazhendhi, Chitosan nanopolymers: An overview of drug delivery against cancer, *Int. J. Biol. Macromol.*, 2019, **130**, 727–736.
16 J. Cui, S. B. Adeloju and Y. Wu, Integration of a highly ordered gold nanowires array with glucose oxidase for ultra-sensitive glucose detection, *Anal. Chim. Acta*, 2014, **809**, 134–140.
17 C. C. Ryan, M. Bardosova and M. E. Pemble, Structural and mechanical properties of a range of chitosan-based hybrid networks loaded with colloidal silica and polystyrene particles, *J. Mater. Sci.*, 2017, **52**, 8338–8347.
18 Y. H. Lin, F. Lu, Y. Tu and Z. F. Ren, Glucose biosensors based on carbon nanotube nanoelectrode ensembles, *Nano Lett.*, 2004, **4**, 191–195.
19 W. Sun, P. Qin, H. Gao, G. Li and K. Jiao, Electrochemical DNA biosensor based on chitosan/nano-V2O5/MWCNTs composite film modified carbon ionic liquid electrode and its application to the LAMP product of Yersinia enterocolitica gene sequence, *Biosens. Bioelectron.*, 2010, **25**, 1264–1270.
20 Q. Wang, B. Zhang, X. Lin and W. Weng, Hybridization biosensor based on the covalent immobilization of probe DNA on chitosan–mutiwalled carbon nanotubes nanocomposite by using glutaraldehyde as an arm linker, *Sens. Actuators, B*, 2011, **156**, 599–605.
21 Y. Liu, M. Wang, F. Zhao, Z. Xu and S. Dong, The direct electron transfer of glucose oxidase and glucose biosensor based on carbon nanotubes/chitosan matrix, *Biosens. Bioelectron.*, 2005, **21**, 984–988.
22 K. R. Ward, N. S. Lawrence, R. S. Hartshorne and R. G. Compton, The theory of cyclic voltammetry of electrochemically heterogeneous surfaces: comparison of different models for surface geometry and applications to highly ordered pyrolytic graphite, *Phys. Chem. Chem. Phys.*, 2012, **14**, 7264–7275.
23 V. Buk, E. Emregul and K. C. Emregul, Alginate copper oxide nano-biocomposite as a novel material for amperometric glucose biosensing, *Mater. Sci. Eng., C*, 2017, **74**, 307–314.
24 Q. Zhu, B. Liang, Y. Cai, Q. Cao, T. Tu, B. Huang, L. Fang and X. Ye, Layer-by-layer chitosan-decorated pristine graphene on screen-printed electrodes by one-step electrodeposition for non-enzymatic hydrogen peroxide sensor, *Talanta*, 2018, **190**, 70–77.
25 M. Sankar, Q. He, M. Morad, J. Pritchard, S. J. Freakley, J. K. Edwards, S. H. Taylor, D. J. Morgan, A. F. Carley, D. W. Knight, C. J. Kiely and G. J. Hutchings, Synthesis of Stable Ligand-free Gold-Palladium Nanoparticles Using a Simple Excess Anion Method, *ACS Nano*, 2012, **6**, 6600–6613.
26 F.-W. Chang, H.-Y. Yu, L. Selva Roselin and H.-C. Yang, Production of hydrogen via partial oxidation of methanol over Au/TiO2 catalysts, *Appl. Catal., A*, 2005, **290**, 138–147.
27 M. P. Casaletto, A. Longo, A. Martorana, A. Prestianni and A. M. Venezia, XPS study of supported gold catalysts: the role of Au-0 and Au+delta species as active sites, *Surf. Interface Anal.*, 2006, **38**, 215–218.
28 J. R. Anusha, C. J. Raj, B.-B. Cho, A. T. Fleming, K.-H. Yu and B. C. Kim, Amperometric glucose biosensor based on glucose oxidase immobilized over chitosan nanoparticles from gladius of Uroteuthis duvauceli, *Sens. Actuators, B*, 2015, **215**, 536–543.
29 S. Deng, G. Jian, J. Lei, Z. Hu and H. Ju, A glucose biosensor based on direct electrochemistry of glucose oxidase immobilized on nitrogen-doped carbon nanotubes, *Biosens. Bioelectron.*, 2009, **25**, 373–377.
30 M. Gu, J. Wang, Y. Tu and J. Di, Fabrication of reagentless glucose biosensors: A comparison of mono-enzyme GOD and bienzyme GOD–HRP systems, *Sens. Actuators, B*, 2010, **148**, 486–491.
31 M. Delvaux, A. Walcarius and S. Demoustier-Champagne, Bienzyme HRP–GOx-modified gold nanoelectrodes for the sensitive amperometric detection of glucose at low overpotentials, *Biosens. Bioelectron.*, 2005, **20**, 1587–1594.
32 X. Chen, J. Zhu, R. Tian and C. Yao, Bienzymatic glucose biosensor based on three dimensional macroporous ionic liquid doped sol–gel organic–inorganic composite, *Sens. Actuators, B*, 2012, **163**, 272–280.
33 C. C. Gong, J. Y. Chen, Y. H. Song, M. Sun, Y. G. Song, Q. H. Guo and L. Wang, A glucose biosensor based on the polymerization of aniline induced by a bio-interphase of glucose oxidase and horseradish peroxidase, *Anal. Methods*, 2016, **8**, 1513–1519.
34 Z. Dai, J. Bao, X. Yang and H. Ju, A bienzyme channeling glucose sensor with a wide concentration range based on co-entrapment of enzymes in SBA-15 mesopores, *Biosens. Bioelectron.*, 2008, **23**, 1070–1076.
35 R. Madhu, B. Devadas, S. M. Chen and M. Rajkumar, An enhanced direct electrochemistry of glucose oxidase at poly (taurine) modified glassy carbon electrode for glucose biosensor, *Anal. Methods*, 2014, **6**, 9053–9058.
36 M. Christwardana, Y. Chung, D.-H. Kim and Y. Kwon, Glucose biofuel cells using the two-step reduction reaction of bienzyme structure as cathodic catalyst, *J. Ind. Eng. Chem.*, 2019, **71**, 435–444.
37 J. Vlasits, C. Jakopitsch, M. Schwanninger, P. Holubar and C. Obinger, Hydrogen peroxide oxidation by catalase-peroxidase follows a non-scrambling mechanism, *FEBS Lett.*, 2007, **581**, 320–324.
38 C. J. Baker, K. Deahl, J. Domek and E. W. Orlandi, Scavenging of H2O2 and Production of Oxygen by Horseradish Peroxidase, *Arch. Biochem. Biophys.*, 2000, **382**, 232–237.
39 S. Alim, A. K. M. Kafi, J. Rajan and M. M. Yusoff, Application of polymerized multiporous nanofiber of SnO2 for designing a bienzyme glucose biosensor based

on HRP/GOx, *Int. J. Biol. Macromol.*, 2019, **123**, 1028–1034.

40 L. D. Zhu, R. L. Yang, J. G. Zhai and C. Y. Tian, Bienzymatic glucose biosensor based on co-immobilization of peroxidase and glucose oxidase on a carbon nanotubes electrode, *Biosens. Bioelectron.*, 2007, **23**, 528–535.

41 Y. Y. Sun, Y. Bai, W. W. Yang and C. Q. Sun, Controlled multilayer films of sulfonate-capped gold nanoparticles/thionine used for construction of a reagentless bienzymatic glucose biosensor, *Electrochim. Acta*, 2007, **52**, 7352–7361.

42 L. Coche-Guérente, S. Cosnier and P. Labbé, Sol–Gel Derived Composite Materials for the Construction of Oxidase/Peroxidase Mediatorless Biosensors, *Chem. Mater.*, 1997, **9**, 1348–1352.

43 F. Tian and G. Zhu, Bienzymatic amperometric biosensor for glucose based on polypyrrole/ceramic carbon as electrode material, *Anal. Chim. Acta*, 2002, **451**, 251–258.

44 W. J. Wang, F. Wang, Y. L. Yao, S. S. Hu and K. K. Shiu, Amperometric bienzyme glucose biosensor based on carbon nanotube modified electrode with electropolymerized poly(toluidine blue O) film, *Electrochim. Acta*, 2010, **55**, 7055–7060.

45 D. R. S. Jeykumari and S. S. Narayanan, Functionalized carbon nanotube-bienzyme biocomposite for amperometric sensing, *Carbon*, 2009, **47**, 957–966.

46 P. Yang, L. Wang, Q. Wu, Z. Chen and X. Lin, A method for determination of glucose by an amperometric bienzyme biosensor based on silver nanocubes modified Au electrode, *Sens. Actuators, B*, 2014, **194**, 71–78.

47 X. Chen, J. Zhu, Z. Chen, C. Xu, Y. Wang and C. Yao, A novel bienzyme glucose biosensor based on three-layer Au–Fe_3O_4@SiO_2 magnetic nanocomposite, *Sens. Actuators, B*, 2011, **159**, 220–228.

48 F. Li, Z. Wang, W. Chen and S. Zhang, A simple strategy for one-step construction of bienzyme biosensor by *in situ* formation of biocomposite film through electrodeposition, *Biosens. Bioelectron.*, 2009, **24**, 3030–3035.

49 Q. L. Sheng and J. B. Zheng, Bienzyme system for the biocatalyzed deposition of polyaniline templated by multiwalled carbon nanotubes: A biosensor design, *Biosens. Bioelectron.*, 2009, **24**, 1621–1628.

50 D. R. S. Jeykumari and S. S. Narayanan, Fabrication of bienzyme nanobiocomposite electrode using functionalized carbon nanotubes for biosensing applications, *Biosens. Bioelectron.*, 2008, **23**, 1686–1693.